Available online at www.sciencedirect.com
SCIENCE DIRECT®
C. R. Mecanique 332 (2004) 353–360
COMPTES RENDUS MECANIQUE

Microgravity and Transfer/Critical fluids

Unsteady two-dimensional convection in a bottom heated supercritical fluid

Isabelle Raspo [a,*], Bernard Zappoli [b], Patrick Bontoux [a]

[a] *Modélisation et simulation numérique en mécanique (MSNM), F.R.E. 2405 CNRS I.M.T., La Jetée, technopôle de Château Gombert, 38, rue Frédéric Joliot Curie, 13451 Marseille cedex 20, France*

[b] *Centre national d'études spatiales (CNES), établissement de Toulouse, 18, avenue Edouard Belin, 31401 Toulouse cedex, France*

Available online 21 April 2004

Abstract

We consider a closed Rayleigh–Bénard cell containing a fluid near its gas–liquid critical point (CP). Due to the divergence of several physical properties near the CP, large Rayleigh numbers can be obtained even for small temperature differences. In the convective regime, the heat flow which is obtained on long time scales exhibits some characteristics of that observed in turbulent convection in normally compressible fluids: it is composed of plumes in thermal boundary layers, jets on lateral walls and a large-scale flow. Our results show that, as it is the case in turbulent convection, this large-scale flow can suddenly change its orientation. ***To cite this article: I. Raspo et al., C. R. Mecanique 332 (2004).***

Résumé

Convection bidimensionnelle instationnaire dans un fluide supercritique chauffé par le bas. On considère un fluide proche de son point critique liquide–gaz (PC) dans une cellule de Rayleigh–Bénard fermée. Du fait de la divergence de plusieurs propriétés physiques au voisinage du PC, des nombres de Rayleigh importants peuvent être obtenus pour de faibles différences de températures. Dans le régime convectif, le champ thermique obtenu sur les longues échelles de temps présente certaines caractéristiques de celui observé en convection turbulente dans un fluide normalement compressible : il est composé de panaches issus des couches limites thermiques, de jets le long des parois latérales et d'un écoulement à grande échelle. Nos résultats montrent que, comme en convection turbulente, cet écoulement peut soudain changer d'orientation. ***Pour citer cet article : I. Raspo et al., C. R. Mecanique 332 (2004).***

Keywords: Fluid mechanics; Supercritical fluid; Convective instability; Reversal of large-scale flow

Mots-clés : Mécanique des fluides ; Fluide supercritique ; Instabilité convective ; Changement d'orientation de l'écoulement à grande échelle

* Corresponding author.
E-mail address: isabel@L3m.univ-mrs.fr (I. Raspo).

1631-0721/$ – see front matter
doi:10.1016/j.crme.2004.02.003

Version française abrégée

Au cours des dix dernières années, l'hydrodynamique des fluides supercritiques a fait l'objet d'un très grand nombre d'études théoriques, expérimentales et numériques, en particulier concernant la convection en configuration de Rayleigh–Bénard [2–7]. Du fait de la divergence de la compressibilité isotherme et de l'expansion thermique au voisinage du PC, les fluides supercritiques présentent des comportements spécifiques, tels qu'une homogénéisation rapide de la température par des effets thermoacoustiques (souvent désignés par effet Piston) [8–10]. Dans cet article, on s'intéresse à la convection instationnaire dans une cavité carrée de hauteur $H = 10$ mm contenant du CO_2 initialement au repos, à une température uniforme T_i très légèrement supérieure à la température critique T_c et stratifié à une densité moyenne égale à la densité critique ρ_c. Le fluide est ensuite chauffé par le bas alors que la paroi supérieure demeure à la température initiale et que les parois latérales sont adiabatiques. La distance au PC est évaluée par un petit paramètre $\tau = (T_i - T_c)/T_c \ll 1$ qui est de l'ordre de 10^{-3} dans ce travail. Le problème est traité numériquement en résolvant les équations de Navier–Stokes instationnaires, compressibles, couplées à l'équation d'énergie et à l'équation de van der Waals pour décrire l'état du fluide. La méthode numérique est basée sur une approximation de type volumes finis avec un schéma d'Euler au 1$^{\text{er}}$ ordre pour la discrétisation temporelle et l'algorithme SIMPLER pour traiter le couplage vitesse-pression. L'approximation à faible nombre de Mach [11] est utilisée.

Du fait de la très forte compressibilité et de la très faible diffusivité thermique du fluide supercritique, le chauffage de la paroi inférieure génère l'apparition de trois zones distinctes dans le fluide : deux fines couches limites de diffusion thermique au voisinage des parois chaude et froide et le cœur de la cavité dont la température est augmentée de façon adiabatique par l'effet Piston (Fig. 1, $t = 6{,}9$ s). Lorsque l'épaisseur de la couche limite chaude h_{hot} dépasse une certaine valeur critique, de sorte que le nombre de Rayleigh local Ra défini par (1) devient supérieur à Ra_c ($\cong 1100$), une instabilité convective, se manifestant sous la forme de panaches thermiques, se déclenche dans la couche limite chaude [6]. De même, une instabilité gravitationnelle se développe dans la couche limite froide. L'évolution du système dans le régime convectif qui suit le déclenchement de l'instabilité se fait en deux étapes. Dans un premier temps, la solution des équations est symétrique par rapport à la ligne médiane $x = H/2$ de la cavité (Fig. 1, $t \leqslant 34$ s). Les panaches apparaissant au voisinage de cette ligne médiane grandissent et sont éjectés dans le cœur de la cavité, alors que les panaches générés près des coins sont advectés vers les parois latérales le long desquelles ils remontent (ou descendent pour les panaches issus de la couche limite froide). La compétition entre de grands panaches chauds et froids finit par aboutir à une brisure de la symétrie de la solution. Du fait de la divergence du rapport $\beta_p C_p/\lambda$ près du PC, de grandes valeurs du nombre de Rayleigh global basé sur H et δT (de l'ordre de 10^7–10^8), dans la gamme de celles relevées en convection turbulente, peuvent être obtenues pour des différences de températures δT de quelques mK. L'écoulement qui se développe dans cette seconde période (Fig. 1, $t \geqslant 75{,}5$ s) présente d'ailleurs plusieurs caractéristiques de celui observé en convection turbulente dans les fluides normalement compressibles [1]. Il est composé de panaches issus de fines couches limites de diffusion thermique, de jets sur les parois latérales et d'un écoulement à grande échelle. Cependant, cet écoulement à grande échelle est constitué de plusieurs cellules de convection (Fig. 3) et non d'une unique grande recirculation comme celà est observé dans les fluides normalement compressibles [1,14]. Au cours du temps, l'écoulement à grande échelle peut subir un rapide et brutal changement d'orientation, comme le montre le changement de signe de la circulation $\Gamma(t)$ définie par (2) dans [5] (Fig. 4). Ce phénomène a été également observé dans des expériences sur la convection turbulente dans un fluide normalement compressible [14] et dans des simulations numériques concernant du ^{3}He supercritique en configuration de Rayleigh–Bénard mais dans une cavité plus petite ($H \approx 1$ mm) et dans le cas d'un chauffage par un flux constant [5]. Le changement d'orientation de l'écoulement à grande échelle semble être provoqué par l'arrivée successive sur la paroi supérieure froide de plusieurs grands panaches chauds. Ces panaches accélèrent fortement l'écoulement dans la couche limite froide vers la paroi latérale gauche (Fig. 5(a), $t \geqslant 105$ s) et finissent par provoquer l'apparition d'un grand panache froid qui descend le long de cette paroi latérale avec une vitesse supérieure à celle du fluide sur la paroi latérale droite (Fig. 5(b), $t \geqslant 122$ s), engendrant un changement global d'orientation de l'écoulement.

1. Introduction

Hydrodynamics of supercritical fluids motivated a significant number of theoretical, experimental and numerical studies during the past ten years, especially concerning the Rayleigh–Bénard problem [2–7]. The divergence of isothermal compressibility and thermal expansion near the CP leads to specific behaviours of supercritical fluids, such as a fast heat equilibration induced by thermoacoustic effects (the so-called Piston Effect) [8–10]. In the same way, large Rayleigh numbers, in the range of turbulent convection, can be obtained even for small temperature differences between the bottom and top walls and for small cavities. The major part of the previous studies were performed in very small cavities (height of about one millimeter) and mainly for supercritical Helium. In this paper, we present some numerical results about the heat flow of supercritical CO_2 in a square Rayleigh–Bénard cell. We discuss in particular its characteristics on long time scales and its similarities with heat flow observed in turbulent convection for normally compressible fluids.

2. Physical model and numerical approach

We consider a 2D square cavity of height $H = 10$ mm which is filled with CO_2 set above its critical point. The fluid is initially at rest, in thermodynamic equilibrium at a uniform temperature T_i which is slightly larger than the critical temperature $T_c = 304.13$ K, and stratified with a mean density equal to the critical density $\rho_c = 467.8\ \mathrm{kg\,m^{-3}}$. Then, the temperature of the bottom wall is raised during 1 s up to the desired temperature $T_{\mathrm{hot}} = T_i + \delta T$, whereas the top wall is kept at the initial temperature and the lateral walls are adiabatic. The distance to the CP is therefore measured by the small parameter $\tau = (T_i - T_c)/T_c \ll 1$.

The flow is governed by the unsteady 2D Navier–Stokes equations coupled with the energy equation and written for a Newtonian, viscous, compressible and heat conducting fluid. The state of the fluid is supposed to be described by the van der Waals equation that takes into account implicitly the divergence of the isothermal compressibility χ_T, of the thermal expansion coefficient β_p and of the heat capacity at constant pressure C_p near the CP. The model is completed by assuming that the dynamic viscosity and the heat capacity at constant volume are constant and equal to their values far from the CP and by introducing the law $\lambda = \lambda_0(1 + \Lambda(T/T_c - 1)^{-0.5})$ (with $\Lambda = 0.75$ and λ_0 the value far from the CP) in order to represent the divergence of the thermal conductivity near the CP. More details about the model can be found in [6].

The governing equations are solved by a finite volume method using a power-law scheme and a first order Euler scheme for time discretization. The coupling between the velocity field and the pressure in the Navier–Stokes equations is solved through the SIMPLER algorithm. A non-uniform 121×121 staggered mesh which is refined near the boundaries is used in order to accurately describe the boundary layers developing in the vicinity to the top and bottom walls. Finally, a low Mach number approximation [11] is used since the acoustic wave description is not needed.

3. Results

The results presented below were obtained for distances to the CP $T_i - T_c = 1$ K ($\tau = 3.3 \times 10^{-3}$) and $T_i - T_c = 0.5$ K ($\tau = 1.6 \times 10^{-3}$) and temperature differences $\delta T = 0.3$ mK and $\delta T = 2.5$ mK. Although the purpose of the present paper is the study of the characteristics of the heat flow on long time scales, we briefly describe the system evolution just after the beginning of bottom wall heating and after the convection onset. A detailed description can be found in [6]. Due to the high compressibility and the very small thermal diffusivity of the supercritical fluid, the heating of the bottom wall induces the appearance of three distinct zones in the fluid layer: two very thin thermal boundary layers near the bottom and top walls, in which diffusion realizes heat transfer, and the bulk of the cavity which temperature is homogeneously increased by thermoacoustic effects (Fig. 1, $t = 6.9$ s).

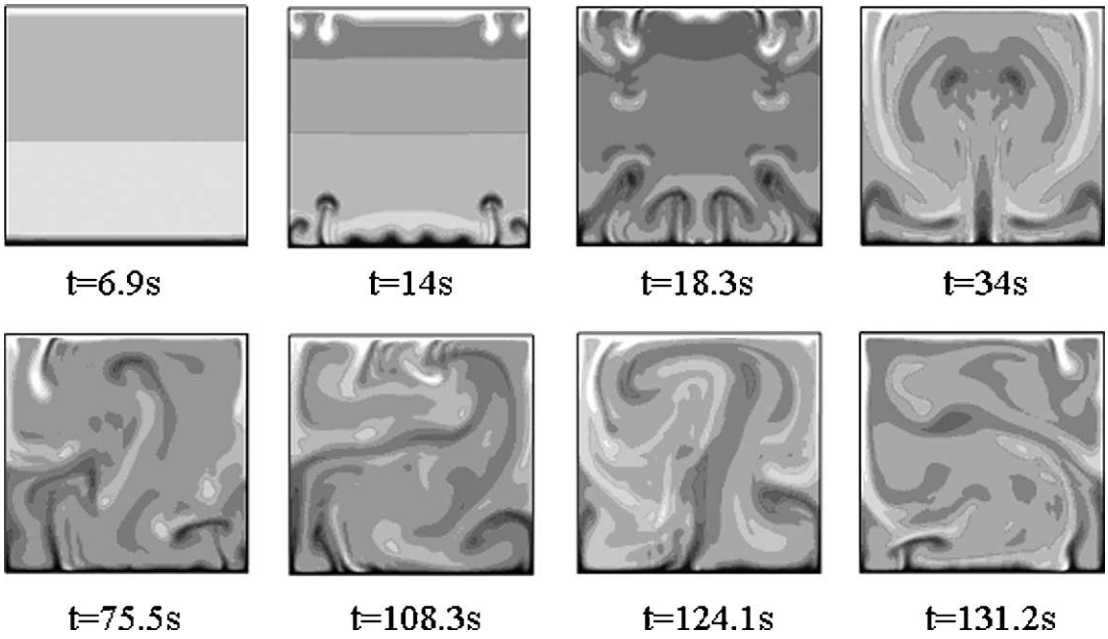

Fig. 1. Instantaneous temperature fields for $\tau = 3.3 \times 10^{-3}$ and $\delta T = 2.5$ mK.

Fig. 1. Champs de température instantanés pour $\tau = 3{,}3 \times 10^{-3}$ et $\delta T = 2{,}5$ mK.

When the thickness h_{hot} of the hot boundary layer exceeds some critical value, so that the local Rayleigh number Ra based on this characteristic length exceeds the critical Rayleigh Ra_c ($\cong 1100$), a convective instability occurs in the hot boundary layer. It must be outlined that, as it was showed by Gitterman and Steinberg [12] and Carlès and Ugurtas [4], the Rayleigh number must be defined using the temperature gradient corrected by the adiabatic gradient, which gives:

$$Ra = Ra_{\text{cl}}(1 - a_g h_{\text{hot}}/\delta T_{\text{hot}}) \tag{1}$$

where Ra_{cl} is the classical Rayleigh number, a_g is the adiabatic gradient and δT_{hot} is the temperature difference inside the hot boundary layer. Due to the very large values of β_p and C_p near the CP, large values of this Rayleigh number (ranging from 4300 to 12 102 with increasing δT, when instability is triggered) are obtained, even for the small temperature differences considered in the present work. The convective instability appears in the form of plume structures, the number of which depends on the temperature difference. In the same time, a gravitational instability, appearing also in the form of plumes, occurs in the cold boundary layer. As the CP is approached, the convective instability appears sooner. As time increases, the plumes grow, expand upwards (or downwards for those originating in the cold boundary layer), are expelled from the boundary layers and are replaced by new ones. Then the heat flow evolution can be divided into two stages.

In the first stage, the solution of the governing equations is symmetric with respect to the vertical center line of the cavity (for $t \leqslant 34$ s in Fig. 1). Plumes generated near the centre line grow and are ejected in the cavity bulk. Some large hot plumes can move upwards and hit the top wall ($t = 34$ s in Fig. 1), triggering a Cold Piston Effect [13]. On the other hand, plumes appearing near the corners are advected along towards the sidewalls and move upwards (or downwards for cold plumes) along these walls. However, these hot and cold lateral plumes never reach the opposite wall and interact at about the mid-height of the sidewalls. At a given time, competition between large hot and cold plumes inside the cavity bulk leads to a break of the solution symmetry. This symmetry loss was observed for all the values of δT and τ that we considered, provided that the simulation time was sufficiently long. However, for a fixed value of τ, it occurs much later as δT decreases (for example, for $\tau = 3.3 \times 10^{-3}$, it occurs at

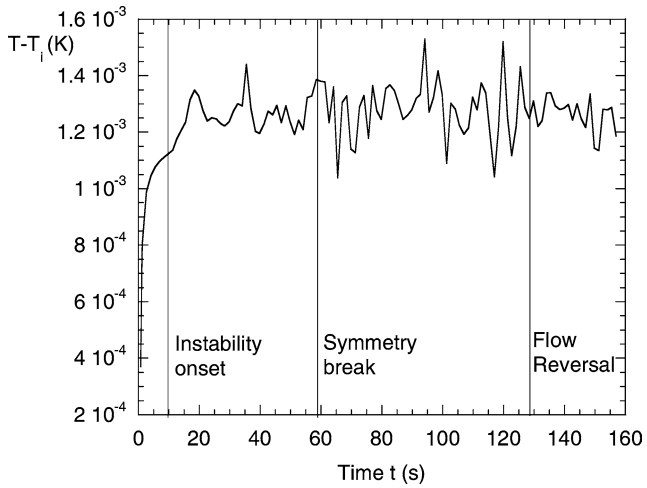

Fig. 2. Evolution of temperature inside the cavity bulk (at $x/H = 0.5,\ y/H = 0.5$) for $\tau = 3.3 \times 10^{-3}$ and $\delta T = 2.5$ mK.

Fig. 2. Evolution de la température dans la cœur de la cavité (en $x/H = 0{,}5$, $y/H = 0{,}5$) pour $\tau = 3{,}3 \times 10^{-3}$ et $\delta T = 2{,}5$ mK.

$t = 59.8$ s for $\delta T = 2.5$ mK and at $t = 197.1$ s for $\delta T = 0.3$ mK), and for a given δT, it occurs sooner as the CP is approached.

In a second stage, the solution of the governing equations is therefore asymmetric (for $t \geqslant 75.5$ s in Fig. 1). The evolution of temperature at the centre of the cavity reveals that the symmetry loss goes with an increase of the characteristic frequency of the solution and of its amplitude (Fig. 2). Due to the divergence of $\beta_p C_p/\lambda$ near the CP, large values of the Rayleigh number for the whole cavity (i.e., based on the height H and on the difference δT), in the range of turbulent convection, are obtained in spite of the small values of the temperature differences that we considered. For example, for $\delta T = 2.5$ mK, the Rayleigh number for the whole cavity is about 5.1×10^7 for $\tau = 3.3 \times 10^{-3}$ and about 1.4×10^8 for $\tau = 1.6 \times 10^{-3}$. Furthermore, in this second stage, the heat flow exhibits several characteristics of that observed in experiments of turbulent convection for normally compressible fluids [1,14]. In particular, it is composed by thermal plumes in the two thin diffusive boundary layers, jets on the sidewalls that are formed by the plumes moving upwards (or downwards) along these walls, and a large-scale flow. However, in experiments for normally compressible fluids, plumes are advected along in opposite directions in the hot and cold boundary layers, form jets on the sidewalls and hit the opposite wall producing a wave there [1]. Therefore, the two diffusive layers are coupled by a large-scale recirculation, which is called the wind [14]. In the present case, the heat flow is somewhat different since the large-scale flow is formed by several convection cells (Fig. 3). As a consequence, plumes are advected along in the same direction in the hot and cold boundary layers. Hence, hot plumes moving upwards along the sidewall never reach the top boundary since they are intercepted by cold plumes moving downwards. The experimental observations for Rayleigh numbers in the range of ours allow us to think that the loss of the solution symmetry is not due to the 2D configuration. Moreover, recent 3D simulations for supercritical CO_2 in a closed Rayleigh–Bénard cell revealed that the solution of the governing equations becomes asymmetric after a transient stage [15].

As time goes by, the large-scale flow can undergo a rapid change in orientation. The same phenomenon was observed in experiments on turbulent convection for normally compressible fluids [14]. On the other hand, Furukawa and Onuki [5] also obtained several successive reversals of the large-scale flow in numerical simulations of the Rayleigh–Bénard problem for supercritical ^{3}He. However, in their case, the cavity was much smaller ($H \approx 1$ mm) and the bottom wall was heated by a constant flux and not by a constant temperature as in our work. Furthermore, their simulations were based on the solution of the Navier–Stokes equations in the Boussinesq

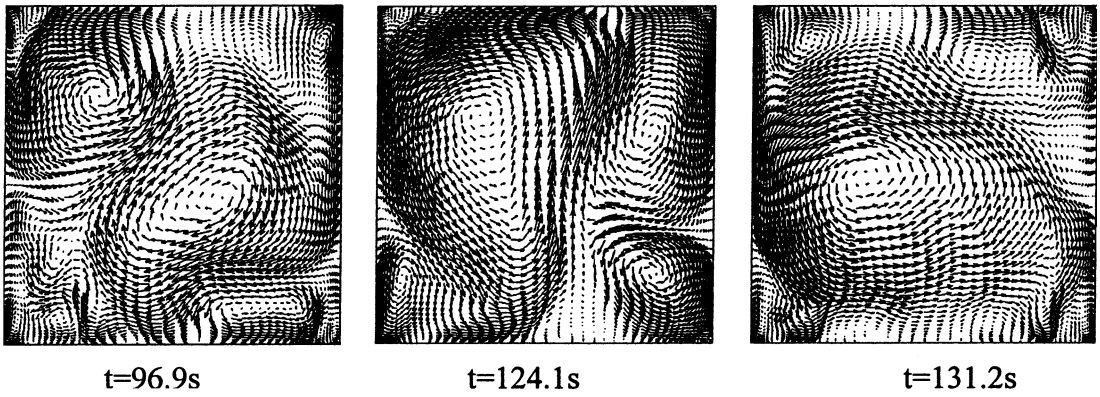

Fig. 3. Instantaneous velocity fields for $\tau = 3.3 \times 10^{-3}$ and $\delta T = 2.5$ mK.

Fig. 3. Champs de vitesse instantanés pour $\tau = 3{,}3 \times 10^{-3}$ et $\delta T = 2{,}5$ mK.

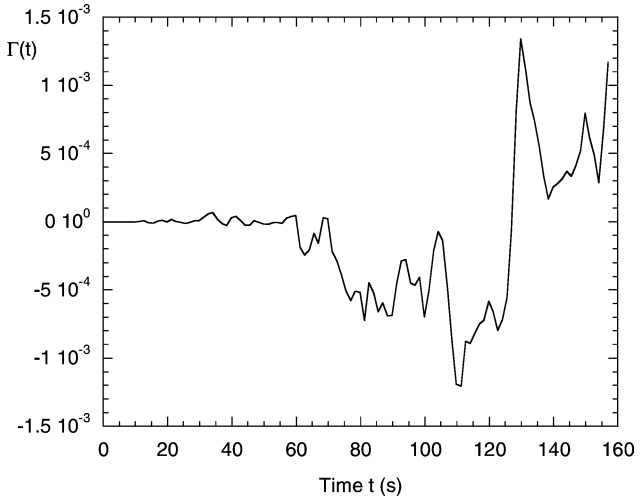

Fig. 4. Evolution of the circulation $\Gamma(t)$ for $\tau = 3.3 \times 10^{-3}$ and $\delta T = 2.5$ mK.

Fig. 4. Evolution de la circulation $\Gamma(t)$ pour $\tau = 3{,}3 \times 10^{-3}$ et $\delta T = 2{,}5$ mK.

approximation coupled with the linearized energy equation. The change of the flow orientation is clearly seen in the evolution of the quantity $\Gamma(t)$ defined in [5] by:

$$\Gamma(t) = \int_d^{H-d} \big[u(x, H-d, t) - u(x, d, t)\big]\,\mathrm{d}x/H + \int_d^{H-d} \big[v(H-d, y, t) - v(d, y, t)\big]\,\mathrm{d}y/H \tag{2}$$

with $d = 0.05H$. This quantity is negative for a clockwise circulation and positive for a counter-clockwise circulation. Fig. 4 shows that, for $\tau = 3.3 \times 10^{-3}$ and $\delta T = 2.5$ mK, the large-scale flow changes its orientation at $t \approx 127$ s since $\Gamma(t)$ changes sign at this time. The reversal of the large-scale flow can also be seen in the velocity patterns shown in Fig. 3 which is very similar to Fig. 13 of [5]: for $t = 96.9$ s, the larger vortex is clockwise whereas it is counter-clockwise for $t = 131.2$ s. We must specify that, for the case shown in Fig. 4, the large-scale flow following the symmetry loss is clockwise, but counter-clockwise flows were also observed just after the symmetry loss for other values of τ and δT (for example for $\tau = 1.6 \times 10^{-3}$ and $\delta T = 2.5$ mK). In [5], Furukawa

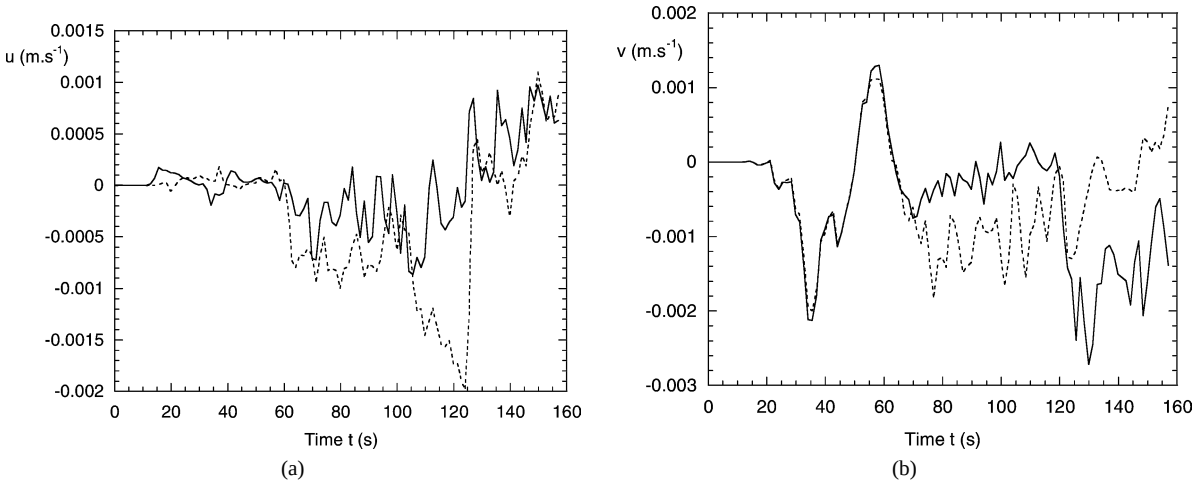

Fig. 5. Evolution of velocity components for $\tau = 3.3 \times 10^{-3}$ and $\delta T = 2.5$ mK: (a) horizontal component u on the centre line ($x/H = 0.5$) at $y/H = 0.03$ (inside the hot boundary layer, solid line) and at $y/H = 0.91$ (inside the cold boundary layer, dotted line); (b) vertical component v at the cavity mid-height ($y/H = 0.5$) at $x/H = 0.05$ (solid line) and at $x/H = 0.95$ (dotted line).

Fig. 5. Evolution des composantes de la vitesse pour $\tau = 3{,}3 \times 10^{-3}$ et $\delta T = 2{,}5$ mK. (a) composante horizontale u sur la ligne centrale de la cavité ($x/H = 0{,}5$) en $y/H = 0{,}03$ (dans la couche limite chaude, trait plain) et en $y/H = 0{,}91$ (dans la couche limite froide, trait pointillé). (b) composante verticale v à mi-hauteur de la cavité ($y/H = 0{,}5$) en $x/H = 0{,}05$ (trait plain) et en $x/H = 0{,}95$ (trait pointillé).

and Onuki explain the reversal of the large-scale flow by the occurrence of a large plume moving through the cavity and suppressing the preexisting primary convection cell, which induces a global orientation change. In the present study, the process leading to the reversal of the large-scale flow can be described as follows. At the time $t \approx 105$ s, several successive large hot plumes move upwards along the left sidewall and, after being deviated by downward cold plumes, hit the top wall near the middle $x/H = 0.5$, driving out cold fluid towards the left sidewall. These successive hot plumes gradually accelerate the fluid inside the cold boundary layer, which is revealed by the strong increase of the horizontal velocity in Fig. 5(a). Then, at time $t = 122$ s, a very large hot plume rapidly grows inside the cavity bulk, hits once again the top wall and accelerates even more the fluid inside the cold boundary layer, inducing the occurrence of a large downward cold plume along the left sidewall. At this time, the velocity of the downward fluid becomes larger near the left sidewall than near the right one (Fig. 5(b)) and induces a global counter-clockwise motion. The evolution of temperature at the centre of the cavity reveals that this reversal of the large-scale flow goes again with a change in the amplitude of the solution (Fig. 2).

4. Conclusion

We presented numerical results concerning unsteady two-dimensional convection in a supercritical fluid under Rayleigh–Bénard configuration. Due to the divergence of the ratio $\beta_p C_p/\lambda$ near the CP, large values of the Rayleigh number based on the cavity height, in the range of turbulent convection, are obtained in spite of the small values of the temperature differences that we considered. We showed that the heat flow for long time scales exhibits several characteristics of those obtained in the turbulent regime. However, in the present case, the large-scale flow consists of several convection cells and not of a large unique recirculation. Our results showed also that the large-scale flow can undergo a rapid change in orientation, as it is the case in turbulent convection. This phenomenon seems to be provoked by the occurrence of successive very large hot plumes which create disequilibrium between fluid velocities inside the cold and hot boundary layers. Computations are performed now in order to check if the reversal of the large-scale flow is generated by the same process for other values of τ and δT. In addition, three-dimensional

simulations are also carried out as a continuation of the preliminary results reported in [15] in order to check the influence of the 2D configuration.

Acknowledgement

The authors gratefully acknowledge support from the Centre National d'Études Spatiales (CNES), the Centre National de la Recherche Scientifique (CNRS) and the IDRIS Computing Center (Orsay, France).

References

[1] L.P. Kadanoff, Turbulent heat flow: Structures and scaling, Phys. Today 54 (8) (2001) 34–39.
[2] M. Assenheimer, V. Steinberg, Rayleigh–Bénard convection near the gas–liquid critical point, Phys. Rev. Lett. 70 (25) (1993) 3888–3891.
[3] A.B. Kogan, H. Meyer, Heat transfer and convection onset in a compressible fluid: ^{3}He near the critical point, Phys. Rev. E 63 (2001) 056310.
[4] P. Carlès, B. Ugurtas, The onset of free convection near the liquid-vapour critical point. Part I: Stationary initial state, Physica A 126 (1999) 69–82.
[5] A. Furukawa, A. Onuki, Convective heat transport in compressible fluids, Phys. Rev. E 66 (2002) 016302.
[6] S. Amiroudine, P. Bontoux, P. Larroudé, B. Gilly, B. Zappoli, Direct numerical simulation of instabilities in a two-dimensional near-critical fluid layer heated from below, J. Fluid. Mech. 442 (2001) 119–140.
[7] S. Amiroudine, B. Zappoli, Piston effect induced thermal oscillations at the Rayleigh–Bénard threshold in supercritical ^{3}He, Phys. Rev. Lett. 90 (2003) 105303.
[8] H. Boukari, J.N. Shaumeyer, M.E. Briggs, R.W. Gammon, Critical speeding up in pure fluids, Phys. Rev. A 41 (1990) 2260–2263.
[9] A. Onuki, H. Hao, R.A. Ferrell, Fast adiabatic equilibration in a single-component fluid near the liquid-vapor critical point, Phys. Rev. A 41 (1990) 2256–2259.
[10] B. Zappoli, D. Bailly, Y. Garrabos, B. Le Neindre, P. Guenoun, D. Beysens, Anomalous heat transport by the piston effect in supercritical fluids under zero gravity, Phys. Rev. A 41 (1990) 2264–2267.
[11] S. Paolucci, On the filtering of sound from the Navier–Stokes equations, Sandia National Laboratories Report SAND82-8257, 1982.
[12] M. Gitterman, V.A. Steinberg, Criteria of occurrence of free convection in a compressible viscous heat-conducting fluid, J. Appl. Math. Mech. 34 (2) (1971) 305–311.
[13] B. Zappoli, A. Jounet, S. Amiroudine, K. Mojtabi, Thermoacoustic heating and cooling in near-critical fluids in the presence of a thermal plume, J. Fluid Mech. 388 (1999) 389–409.
[14] J.J. Niemela, L. Skrbek, K.R. Sreenivasan, R.J. Donnelly, The wind in confined thermal convection, J. Fluid Mech. 449 (2001) 169–178.
[15] G. Accary, I. Raspo, P. Bontoux, B. Zappoli, Three-dimensional Rayleigh–Bénard instability in a supercritical fluid, C. R. Mécanique, in press.